Molecular Therapy
Methods & Clinical Development
Original Article

Cathepsin B inhibition blocks amyloidogenesis in the mouse models of neurological lysosomal diseases MPS IIIC and sialidosis

Gustavo M. Viana,[1,3] Xuefang Pan,[1,3] Shuxian Fan,[1,2] TianMeng Xu,[1,2] Alexandra Wyatt,[1] and Alexey V. Pshezhetsky[1,2]

[1]Division of Medical Genetics, Centre Hospitalier Universitaire (CHU) Ste-Justine Research Centre, Montreal, QC H3A 0C7, Canada; [2]Department of Anatomy and Cell Biology, McGill University, Montreal, QC H3T 1C5, Canada

Neuronal accumulation of amyloid aggregates is a hallmark of brain pathology in neurological lysosomal storage diseases (LSDs), including mucopolysaccharidoses (MPS); however, the molecular mechanism underlying this pathology has not been understood. We demonstrate that elevated lysosomal cathepsin B (CTSB) levels and CTSB leakage to the cytoplasm triggers amyloidogenesis in two neurological LSDs. CTSB levels were elevated 3- to 5-fold in the cortices of mouse models of MPS IIIC (*Hgsnat-Geo* and *Hgsnat*^{P304L}) and sialidosis (*Neu1*$^{\Delta Ex3}$), as well as in cortical samples of MPS I, IIIA, IIIC, and IIID patients. CTSB was found in the cytoplasm of pyramidal layer IV-V cortical neurons containing thioflavin-S$^+$, β-amyloid$^+$ aggregates consistent with a pro-senile phenotype. In contrast, CTSB-deficient MPS IIIC (*Hgsnat*^{P304L}/*Ctsb*$^{-/-}$) mice as well as *Hgsnat*^{P304L} and *Neu1*$^{\Delta Ex3}$ mice chronically treated with irreversible brain-penetrable CTSB inhibitor E64 showed a drastic reduction in neuronal thioflavin-S$^+$/APP$^+$ deposits. Neurons of *Hgsnat*^{P304L}/*Ctsb*$^{-/-}$ mice and E64-treated *Hgsnat*^{P304L} mice also showed reduced levels of P62$^+$, LC3$^+$ puncta, G_{M2} ganglioside, and misfolded subunit C of mitochondrial ATP synthase, consistent with restored autophagy. E64 treatment also rescued hyperactivity and reduced anxiety in *Hgsnat*^{P304L} mice, implying that CTSB may become a novel pharmacological target for MPS III and similar LSDs.

INTRODUCTION

About two-thirds of patients affected with lysosomal storage diseases (LSDs), inherited metabolic disorders caused by lysosomal dysfunction, display neurological symptoms.[1] Although the severity of CNS pathology and specific pathological signs can be different for different LSDs, several pathological cascades were found to be common. This includes neuroimmune response, manifesting with population of the brain by activated macrophages/microglia and astrocytes expressing pro-inflammatory cytokines; neuronal death affecting essential brain areas such as cortex, hippocampus and cerebellum; loss of myelin; and neuronal dysfunction affecting synaptic transmission and synaptogenesis (reviewed in reference[2]). Several common biomarkers of CNS pathology in neurological LSDs, most notably amyloidogenesis and accumulation of neuronal misfolded protein aggregates, neurofibrillary tangles, and lipofuscin bodies, are also shared with adult neurogenerative disorders, such as Parkinson disease, Alzheimer disease (AD), frontotemporal dementia, dementia with Lewy bodies, and others. In addition, the prevalence of common neurogenerative diseases is often associated with the deficiency or haploinsufficiency of lysosomal hydrolases such as glucocerebrosidase, acid sphingomyelinase, and others, suggesting the existence of shared pathophysiological mechanisms with LSDs such as defects in the autophagic pathway, essential for removal of misfolded and aggregated proteins or damaged organelles.[3–7]

Intraneuronal aggregates of β-amyloid peptides have been observed in multiple classes of LSDs with different types of primary biochemical defects and storage materials. In particular, it has been detected in neurological mucopolysaccharidoses (MPS) caused by deficiency of lysosomal enzymes involved in the degradation of heparan sulfate (HS).[8] In the mouse models of MPS type III (Sanfilippo disease), caused by the deficiency of four lysosomal enzymes specifically involved in HS catabolism, amyloid aggregates were predominantly found in the pyramidal cortical neurons, which also accumulated misfolded mitochondrial proteins (mainly subunit C of mitochondrial ATP synthase [SCMAS]), phosphorylated tau, and secondary metabolites such as cholesterol and simple gangliosides (e.g., G_{M2}, G_{M3}).[9–14] This has been proposed to cause an intracellular metabolic imbalance and, consequently, loss of neuronal viability.[12,15,16] The neurons containing β-amyloid deposits were also strongly positive for the presence of P62$^+$ and LC3$^+$ puncta, the markers of impaired autophagy; however, the exact mechanistic link between the two phenomena has not been established and requires further investigation (reviewed in reference[17]). In particular, inhibition of autophagy and lysosomal genes expression corrected several pathological features in MPS III cells and the MPS IIIB

Received 13 May 2024; accepted 7 February 2025;
https://doi.org/10.1016/j.omtm.2025.101432.

[3]These authors contributed equally

Correspondence: Alexey V. Pshezhetsky, Division of Medical Genetics, CHU Ste-Justine Research Centre, Montreal, QC H3A 0C7, Canada.
E-mail: alexei.pchejetski@umontreal.ca

model,[18] as well as in MPS II mice[19]; however, induction of autophagy and lysosomal genes expression ameliorated the phenotype of MPS IIIA mice.[20] Notably, accumulation of β-amyloid aggregates was also described in the mouse model of a neurological LSD sialidosis, caused by genetic deficiency of neuraminidase 1 (NEU1).[21] The authors speculated that NEU1 deficiency caused oversialylation of β-amyloid peptides and their increased secretion from the cell leading to the formation of amyloid plaques.[21]

The internalization and subsequent processing of the amyloid precursor protein (APP) by β-secretase 1 and γ-secretase have been recognized as the main mechanism underlying the generation of β-amyloid peptides in AD.[22–24] However, other proteases and, in particular, lysosomal cathepsin B (CTSB) also play a role in amyloidogenic APP processing.[25–29] Importantly, CTSB was also found to be an essential component of the inflammasome, required for the inflammatory activation of microglia,[30–32] and one of the key enzymes in the regulation of autophagic flux.[33] Our previous work showed that in pyramidal cortical neurons of MPS I (*Idua*$^{-/-}$) mice, increased levels of CTSB and its leakage from lysosomes to the cytoplasm coincided with amyloidogenic APP processing and accumulation of β-amyloid aggregates.[34]

In the present study, we show that genetic inactivation of CTSB completely abolishes accumulation of β-amyloid aggregates in the pyramidal cortical neurons of the MPS IIIC *Hgsnat*^{P304L} mouse model. Moreover, we demonstrate that chronic treatment with irreversible brain-penetrable CTSB inhibitor E64 causes a similar effect in both MPS IIIC and sialidosis mice. The treatment also improves behavioral deficits and CNS lesions in MPS IIIC mice, suggesting that CTSB may become a novel pharmacological target for neurological LSDs.

RESULTS

Cathepsin B is overexpressed and shows abnormal cytoplasmic localization in pyramidal neurons of cortical layers IV-V in mouse models of MPS IIIC and sialidosis

To test whether levels of CTSB are increased in the cortical neurons of neurological LSDs manifesting with amyloidogenesis, we analyzed levels of CTSB protein and activity in cortices of two mouse models of MPS IIIC, the HGSNAT knockout (KO; *Hgsnat-Geo*) and knockin (*Hgsnat*^{P304L}) mouse strains and a mouse model of sialidosis (*Neu1*$^{\Delta Ex3}$) that we have previously developed and characterized.[13,35,36] MPS IIIC patients accumulate HS, while sialidosis patients accumulate sialylated glycoproteins and oligosaccharides.[37,38]

Mice were sacrificed at the age corresponding to the advanced stage of CNS pathology (6 months for MPS IIIC models, 4 months for sialidosis), their brains dissected, homogenized, and analyzed by immunoblotting to assess levels of CTSB protein. Our results (Figures 1A and 1B) indicated that in all three LSD models the levels of the mature 25-kDa form of CTSB were significantly increased from ∼3-fold (in MPS IIIC) to ∼5-fold (in sialidosis). Enzymatic CTSB activity, measured in cortex homogenates with a specific fluorogenic substrate, Z-Arg-Arg-AMC, showed a similar increase (Figure 1C).

We further analyzed sagittal brain sections of wild-type (WT) and *Hgsnat-Geo* mice by immunohistochemistry to identify brain regions with the highest increase in the levels of CTSB. An increased intensity of CTSB staining in *Hgsnat-Geo* mice was observed mainly in somatosensory brain cortex, while in other areas, such as hippocampus, neurons showed levels of CTSB immunoreactivity similar to those in WT animals (Figure S1). Similar results were observed in other models, which prompted us to select isocortex as the main region of interest. Furthermore, immunofluorescent analysis of cortex tissues of all three mouse models revealed that CTSB was drastically increased in the pyramidal neurons of deep (IV-V) layers of the somatosensory cortex (Figure 1D).

CTSB levels and localization in different types of cortical cells was further studied by IHC. For this, the brain sections of WT, *Hgsnat-Geo*, *Hgsnat*^{P304L}, and *Neu1*$^{\Delta Ex3}$ mice were labeled with antibodies against CTSB and protein markers of neurons (NeuN), astrocytes (glial fibrillary acidic protein [GFAP]), and activated microglia (CD11b) (Figure S2). In all studied brains of MPS IIIC and sialidosis mice, we found a drastic increase in CTSB levels in the NeuN^{+} pyramidal layer IV-V neurons. The same cells also contained the highest levels of misfolded SCMAS, as well as amyloid β^{+}/thioflavin-S^{+} aggregates previously identified as the robust markers of CNS pathology in neurological LSDs.[13,35] Levels of GFAP^{+} astrocytes in the same area were drastically increased in all models, indicative of astrocytosis; however, no co-localization was found for CTSB^{+} and GFAP^{+} cells, suggesting that CTSB biogenesis in the astrocytes is not increased. CD11b labeling revealed multiple cells, which were also CTSB^{+} and found in proximity to NeuN^{+} areas, indicating that the majority of activated microglia were perineuronal and that, similar to pyramidal neurons, they overexpressed CTSB.

Previously, we have shown in the cortical neurons of the MPS I mouse model that increased CTSB levels coincided with its cytoplasmic localization, suggesting that the enzyme was leaking from the lysosomes to the cytoplasm.[34] In the present study, diffused CTSB intracellular pattern and reduced co-localization with lysosome-associated membrane protein 1 (LAMP-1) was also observed in the cortical neurons of *Hgsnat-Geo*, *Hgsnat*^{P304L}, and sialidosis mice (Figure 2A), which could be a consequence of the lysosomal membrane permeabilization. To verify this, we have stained brain sections with fluorescein isothiocyanate-labeled GAL3C, the recombinant soluble lectin domain of human galectin-3 (Figure 2B). Previously, lysosomal recruitment of this galactose-specific lectin was shown to be associated with the lost integrity of lysosomal membranes, resulting in leakage of galactose-containing proteins into the cytoplasm, and thought to be a part of the mechanism aimed at the isolation of leaking lysosomes and their further elimination by autophagocytosis.[39] The pyramidal neurons in WT brains were GAL3C^{-}, suggestive of the preserved integrity of lysosomal membranes. In contrast, the neurons in the brains of *Hgsnat-Geo*, *Hgsnat*^{P304L}, and sialidosis mice contained GAL3C^{+} perinuclear puncta, which partially co-localized with CTSB, consistent with the leakage of the lysosomal content to the cytoplasm.

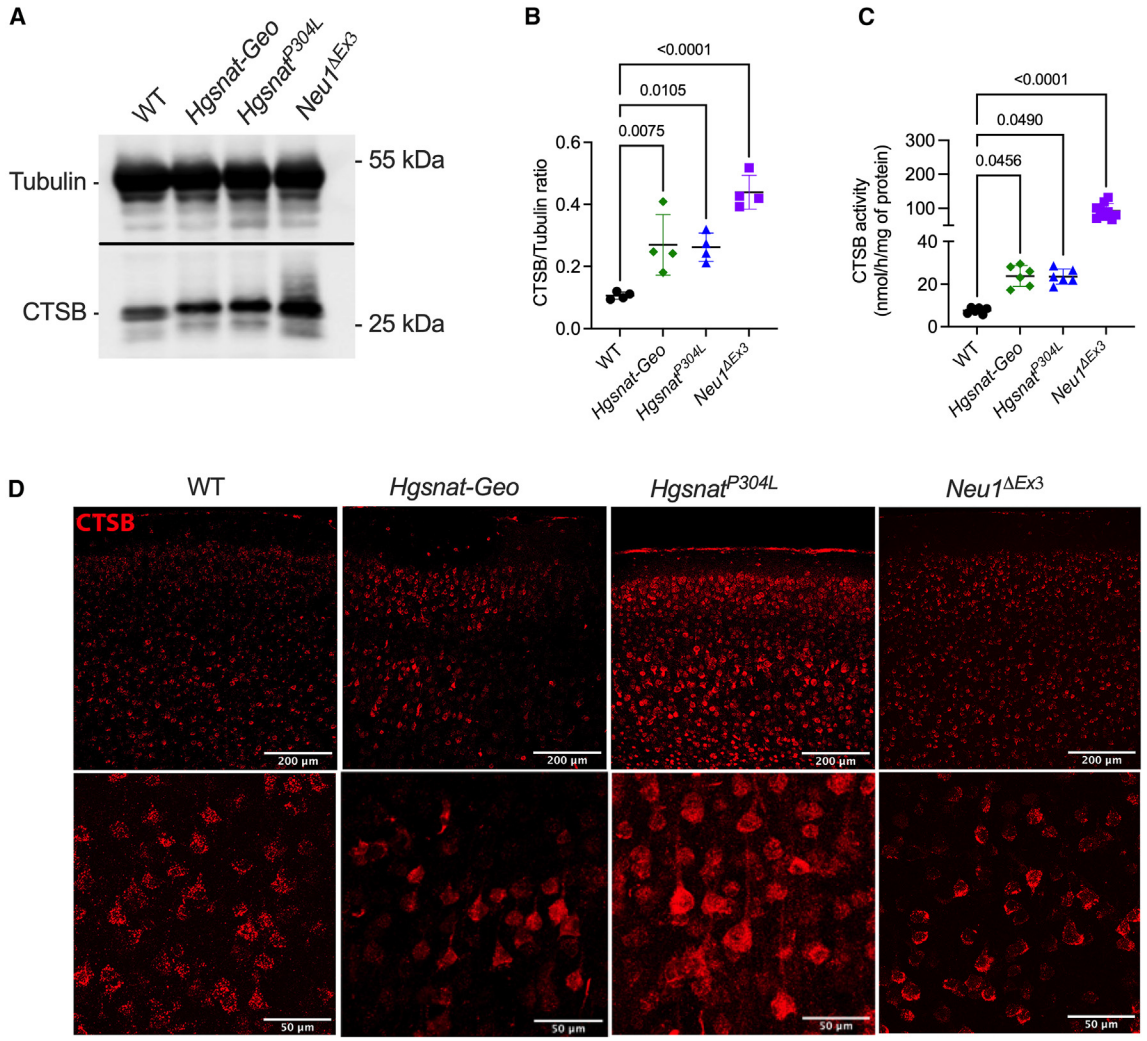

Figure 1. Increased CTSB levels in brain cortices of MPS IIIC and sialidosis mice

(A) Representative immunoblot images and (B) quantitative analysis of CTSB band intensities normalized by tubulin. (C) Enzymatic activity of CTSB in brain cortex lysates measured using the Z-Arg-Arg-AMC substrate. (D) Representative confocal images of brain cortex (layers IV-V) of WT, *Hgsnat-Geo*, *Hgsnat*^{P304L}, and *Neu1*$^{\Delta Ex3}$ mice, showing immunolabeling for CTSB (red), analyzed at lower magnification (top) and higher magnification (digital zoom of the layer V, bottom). Individual results, means, and SDs from four to nine mice per genotype are shown. *p* values were calculated using ANOVA with the Brown-Forsythe post hoc test. Scale bars, 200 µm (top) and 20 µm (bottom).

The increased cytoplasmic localization of CTSB in the brain cells of *Hgsnat*^{P304L} mice was further confirmed by differential centrifugation. Pooled freshly harvested brain tissues of three WT and three *Hgsnat*^{P304L} 6-month-old mice were homogenized in isotonic buffer and separated to post-nuclear supernatant, organellar fraction (containing both mitochondria and lysosomes), and cytosol. The analysis of CTSB protein in the collected fractions by immunoblot (Figures S3A and S3C) revealed a drastic increase in the relative CTSB content in the cytosol fraction obtained from the pooled brains of *Hgsnat*^{P304L} mice (31% of the total amount detected in the post-nuclear supernatant) compared to WT mice of the same age (7.4% of the total amount), consistent with CTSB leakage from the lysosomes to the cytosol. These results also confirmed an increase in the total CTSB levels in the brains of *Hgsnat*^{P304L} compared to WT mice previously revealed by enzyme activity assays and immunofluorescence microscopy (Figure S3B).

Increased levels of CTSB are associated with presence of neuronal amyloid deposits and amyloidogenic procession of APP

In the *Hgsnat-Geo*, *Hgsnat*^{P304L}, and *Neu1*$^{\Delta Ex3}$ mouse cortices, pyramidal neurons overexpressing CTSB also showed drastically increased fluorescence staining with thioflavin-S (Figure 3A). Since after binding to β sheet-rich peptide deposits, this dye displays enhanced fluorescence, it is commonly used for detection of misfolded proteins, including amyloid aggregates in the brains of AD

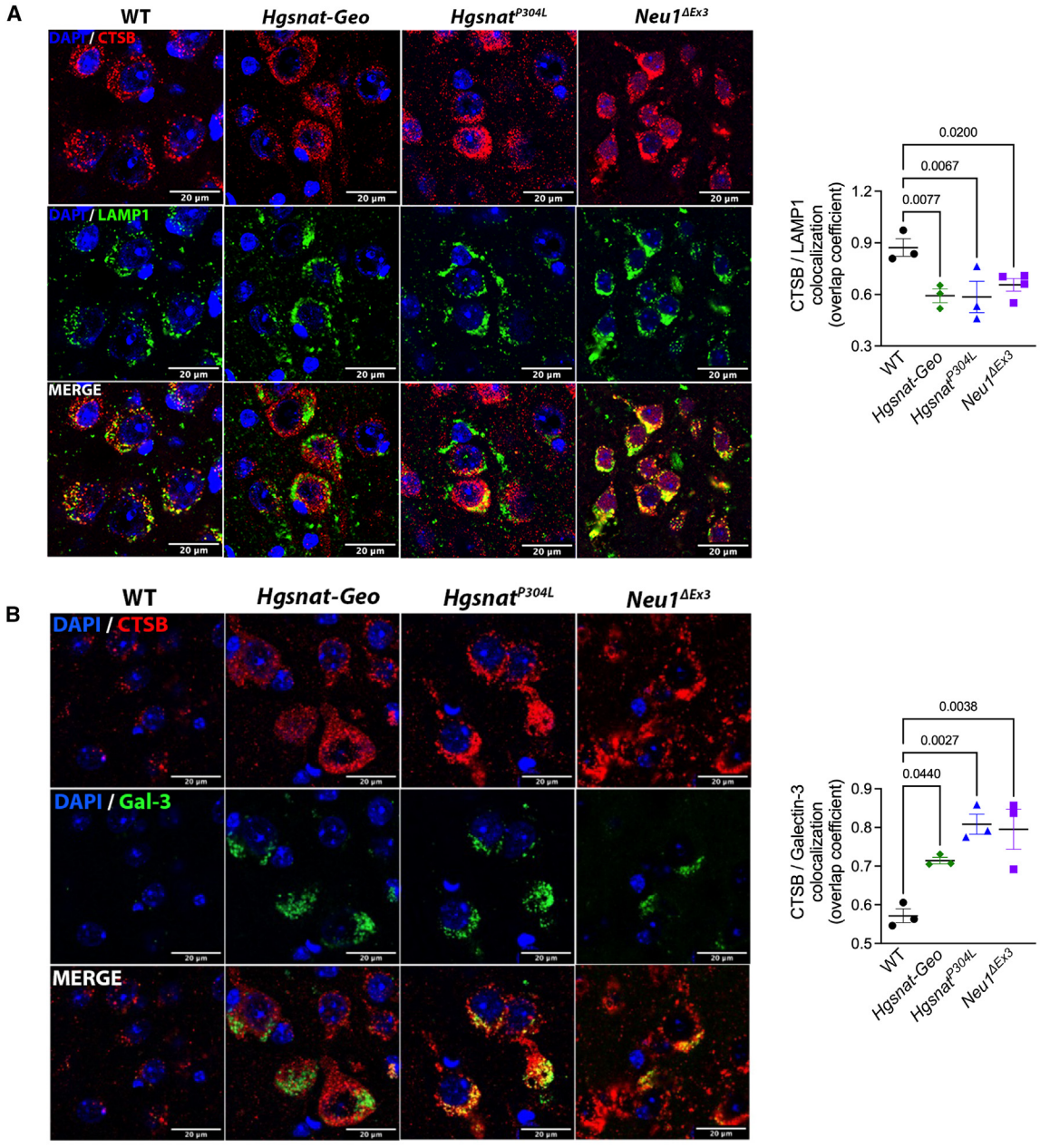

Figure 2. Increased levels of CTSB and its leakage to the cytoplasm in cortical neurons of MPS IIIC and sialidosis mice

Representative confocal microscopy images of brain cortex (layers IV-V) of WT, *Hgsnat-Geo*, *Hgsnat*^{P304L}, and *Neu1*$^{\Delta Ex3}$ mice labeled for (A) CTSB (red) and LAMP-1 (green) or (B) CTSB (red) and galectin-3 (green). DAPI (blue) was used as the nuclear counterstain. Thirty images were analyzed. Graphs show Manders' colocalization coefficient values for CTSB and LAMP-1 or CTSB and galectin-3 measured with ImageJ. Individual data, means, and SDs from three mice per genotype (30 images for each mouse) are shown. *p* values were calculated by ANOVA with Tukey's post hoc test. Scale bars, 20 µm.

patients. In most neurons, thioflavin-S staining co-localized with the areas stained with antibodies against the β-amyloid protein (AP), suggestive of amyloid accumulation in these cells (Figure S4). The levels of the full-length amyloid precursor protein (APP), measured by immunoblot in brain cortex homogenates, were similar for all groups of mice (Figure 3B). In contrast, elevated levels of 16-kDa C-terminal AP fragments (antibodies 1–40 and 1–42 peptides together) were found in *Hgsnat*^{P304L} and *Neu1*$^{\Delta Ex3}$ compared to WT mice, indicative of enhanced amyloidogenic APP processing and pro-senile neuronal phenotype. These data suggest that the massive increase in the cytoplasmic pool of CTSB can be linked to amyloidogenic processing of APP and deposition of β-amyloid aggregates in all three models.

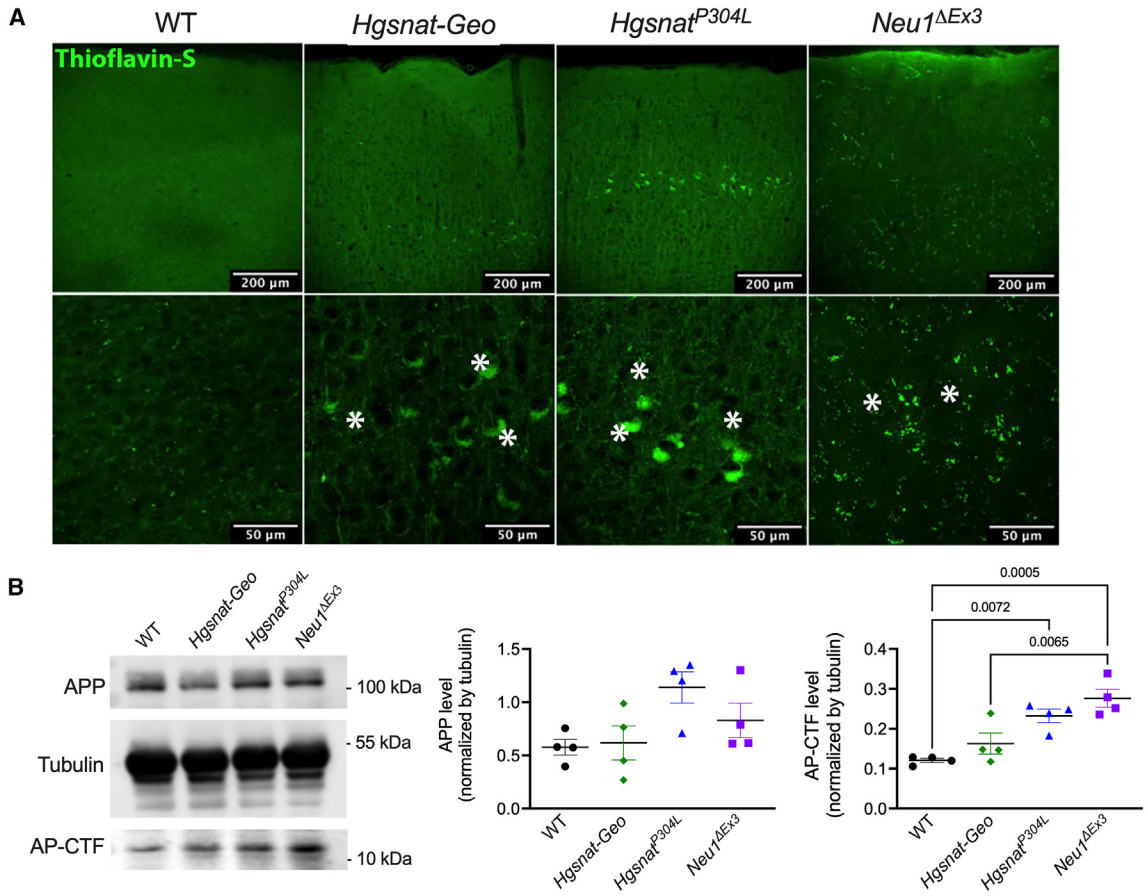

Figure 3. Cortices of MPS IIIC and sialidosis mice contain thioflavin-S$^+$ pyramidal neurons and reveal elevated levels of 16-kDa C-terminal AP fragments
(A) Representative confocal microscopy images of brain cortex of MPS IIIC and sialidosis mice labeled with thioflavin-S. Thioflavin$^+$ deposits in pyramidal layers IV-V neurons are marked with asterisks. Bar graphs: 200 μm (top) and 50 μm (bottom). (B) Immunoblot shows unchanged levels of amyloid precursor protein (APP) but elevated levels of 16-kDa C-terminal AP fragments (AP-CTF) in cortex homogenates of *Hgsnat-Geo*, *Hgsnat*^{P304L}, and *Neu1*$^{\Delta Ex3}$ mice. Graphs show individual results, means, and SDs. *p* values were calculated using ANOVA with Tukey post hoc test; $n = 4$ animals per genotype. Only $p < 0.05$ are shown.

Levels of CTSB activity and protein are increased in cortical tissues of neurological MPS patients

To determine whether the levels of CTSB and amyloid aggregates are also increased in the cortical neurons of patients affected with MPS III and other neurological MPS diseases, we analyzed frozen and paraformaldehyde (PFA)-fixed somatosensory cortex of postmortem tissue, collected at autopsy and donated to the NIH NeuroBioBank. Samples from six MPS patients (MPS I, MPS II, MPS IIIA, MPS IIIC, and two MPS IIID) and six non-MPS controls, matched for age and sex, were examined (project 1071, MPS Synapse). The age, cause of death, sex, race, and available clinical and neuropathological information for the patients and controls are shown in Table S2. All MPS patients had complications from their primary disease and died prematurely (before age 25 years). None of the patients had received enzyme replacement therapy or hematopoietic stem cell transplantation. Enzymatic assays and immunoblotting performed on the frozen tissues confirmed that the CTSB activity and protein levels were significantly increased in cortices of MPS patients compared to controls (Figures 4A and 4B), suggesting that increase in the levels of this enzyme may be a common hallmark for most subtypes of MPS. In turn, staining of fixed cortical slices with thioflavin S showed that most of the patients' tissues (four of five) but none of the controls were positive for the presence of misfolded protein inclusions.

Genetic Ctsb inactivation in *Hgsnat*^{P304L} mice reduces amyloidogenesis, neuronal accumulation of G_{M2}-ganglioside, and neuroinflammation

To reveal a causative relation between the increase in the CTSB levels and accumulation of amyloid aggregates in the cortical neurons, we studied *Hgsnat*^{P304L} mice with genetic depletion of the *Ctsb* gene (*Hgsnat*^{P304L}/*Ctsb*$^{-/-}$). The strain was generated by breeding the *Hgsnat*^{P304L} strain with previously described *Ctsb* KO mice (Jax strain [B6; 129-Ctsbtm1Jde/J]). Analysis of the brain tissues of *Ctsb*$^{-/-}$ and *Hgsnat*^{P304L}/*Ctsb*$^{-/-}$ mice demonstrated an absence of CTSB enzymatic activity (Figure 5A) or immunoreactive material (Figure 5B). *Ctsb*$^{-/-}$ mice do not show increased levels and size of LAMP-2$^+$

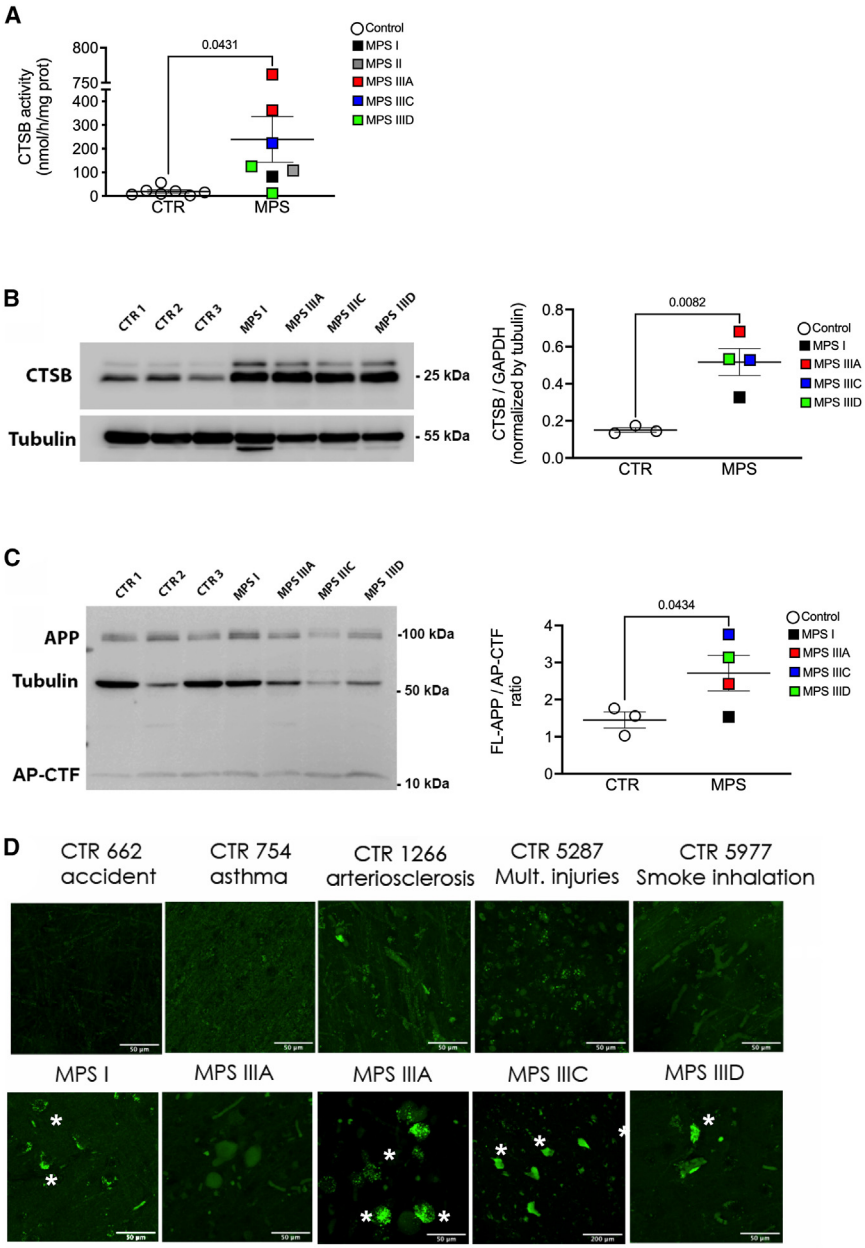

Figure 4. Cortices of MPS patients reveal elevated levels of CTSB activity and protein and contain thioflavin-S^{+} pyramidal neurons and elevated levels of 16-kDa C-terminal AP fragments, suggestive of amyloid accumulation

(A) Enzymatic activity of CTSB in brain cortex lysates was measured using the Z-Arg-Arg-AMC substrate. Individual results, means, and SDs are shown. (B) Immunoblot shows elevated levels of CTSB in cortex homogenates of MPS patients compared to those without MPS (CTR). (C) Immunoblot shows elevated levels of 16-kDa AP-CTF in cortex homogenates of MPS patients. Graphs show individual results, means, and SDs. *p* values were calculated by t test. (D) Representative confocal microscopy images of the brain cortex of MPS patients labeled with thioflavin-S (green) show the presence of misfolded protein deposits (marked with asterisks) undetectable in the cortical samples of age-/sex-matched controls without MPS.

puncta in the neurons, a marker of lysosomal storage (Figure 5C), and they do not display biomarkers of CNS pathology common for neurological LSDs, including astromicrogliosis (Figure 5D). Analysis of CNS pathology in 6-month-old *Hgsnat*^{P304L}/*Ctsb*$^{-/-}$ mice revealed drastically reduced levels of thioflavin-S/β-amyloid double-positive aggregates (Figure 5E) in cortical pyramidal neurons compared to *Hgsnat*^{P304L} mice, demonstrating that depletion of CTSB blocked amyloidogenesis. In addition, the cortical neurons of *Hgsnat*^{P304L}/*Ctsb*$^{-/-}$ mice showed reduced levels of misfolded SCMAS (Figure 5F) and G_{M2} ganglioside (Figure 5G) and did not contain LC3^{+} and P62^{+} puncta, suggesting that CTSB depletion also rescued an autophagy block (Figures 5H and 5K). However, the level of astromicrogliosis in the CTSB-deficient *Hgsnat*^{P304L}/*Ctsb*$^{-/-}$ mice was similar to that in the *Hgsnat*^{P304L} strain (Figure 5D).

Chronic treatment of *Hgsnat*^{P304L} mice with pharmacological CTSB inhibitor E64 rescues behavioral abnormalities and reduces amyloid deposits in cortical pyramidal neurons

Taking advantage of the fact that the brain-permeable irreversible CTSB inhibitor E64 (also known as aloxistatin) is available and does not show toxicity in doses of 1–5 mg/kg body weight (BW), sufficient to inhibit the enzyme in the mouse brain tissues,[40–43] we further tested whether pharmacological CTSB inhibition matches the results of its genetic inactivation in *Hgsnat*^{P304L} mice. As a delivery route, we have chosen intranasal administration, which is non-invasive and showed efficacy in delivery of small (<1,000 Da) molecules to the brain parenchyma.[44] Mice were treated with daily E64 doses of 1 mg/kg BW between the ages of 5 and 6 months—in other words, directly preceding the age when accumulation of amyloidogenic deposits in cortical neurons becomes evident.[35] Mice were then analyzed by an open field (OF) test, instrumental in detecting hyperactivity and reduced anxiety, characteristic of MPS IIIC mice, and sacrificed to analyze CNS pathology. Similar analyses were conducted for untreated *Hgsnat*^{P304L} and *Hgsnat*^{P304L}/*Ctsb*$^{-/-}$ mice, as well as for untreated and treated WT mice of similar age and sex. As expected, untreated 6-month-old *Hgsnat*^{P304L} mice showed an increase in the total travel distance (hyperactivity; Figure 6A) and in the amount of time spent in the

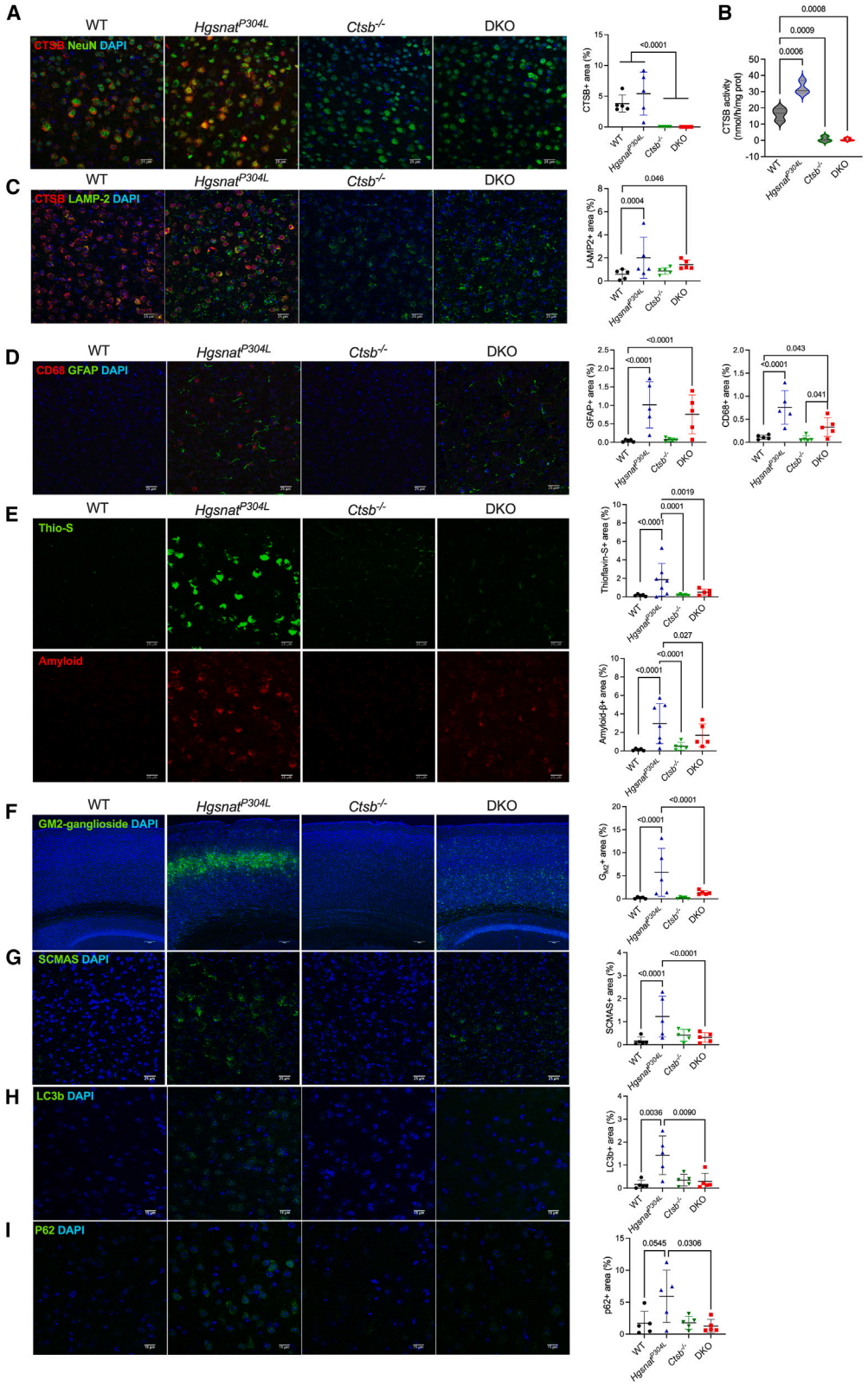

(legend on next page)

central area (reduced anxiety; Figures 6B–6F) compared to WT mice. In contrast, *Hgsnat*^{P304L} mice treated with E64 demonstrated normal behavior in the OF test, similar to the behavior of the control mice. WT mice treated with E64 exhibited behavior undistinguishable from that of untreated WT mice. Somewhat unexpectedly, both *Hgsnat*^{P304L}/*Ctsb*$^{-/-}$ and *Ctsb*$^{-/-}$ mice, similar to untreated *Hgsnat*^{P304L} mice, showed an increase in total distance traveled and time spent/distance traveled in the central area compared to WT mice, consistent with hyperactivity and reduced anxiety.

Analysis of the brain tissues by IHC conducted in 7-month-old mice revealed that, like the *Hgsnat*^{P304L}/*Ctsb*$^{-/-}$ mice, E64-treated *Hgsnat*^{P304L} mice did not contain thioflavin-S^{+} and APP^{+} depositions in cortical neurons (Figure 7A), thus demonstrating that the drug effectively prevented the accumulation of amyloid aggregates. E64-treated *Hgsnat*^{P304L} mice also did not show SCMAS storage (Figure 7B) or LC3^{+} and P62^{+} puncta in cortical pyramidal neurons (Figure 7C), suggesting the drug restored normal autophagy levels.

At the same time, as in CTSB-deficient *Hgsnat*^{P304L}/*Ctsb*$^{-/-}$ mice, the level of astromicrogliosis in the *Hgsnat*^{P304L} mice treated with E64 was similar to that in the untreated *Hgsnat*^{P304L} mice (Figure S5). This was consistent with increased expression levels of pro-inflammatory cytokines macrophage inflammatory protein 1 α (MIP1α) and tumor necrosis factor α (TNF-α) in their brain tissues (Figure S6). However, the expression of interleukin-1β (IL-1β) was normalized in the brains of treated mice.

Chronic treatment of sialidosis mice with E64 reduces amyloid deposits in cortical layer IV-V pyramidal neurons

We further tested whether E64 treatment would also reduce amyloidogenesis in the cortices of sialidosis mice. Since these mice show more aggressive disease progression causing severe debilitation and death by the age of 18–24 weeks,[36] we treated them starting from weaning (∼6 weeks) until the age of 16 weeks, when the mice were sacrificed and their fixed brain tissue cryopreserved to study the accumulation of amyloid deposits in the cortical neurons. This analysis revealed that the β-amyloid/thioflavin-S^{+} aggregates, clearly present in the pyramidal cortical layer IV-V neurons of untreated *Neu1*$^{\Delta Ex3}$ mice, were absent in the brains of both WT and E64-treated *Neu1*$^{\Delta Ex3}$ mice (Figure 8A). Similar to E64-treated MPS IIIC *Hgsnat*^{P304L} mice and MPS IIIC mice with CTSB deficiency (*Hgsnat*^{P304L}/*Ctsb*$^{-/-}$), E64-treated sialidosis mice showed significantly reduced levels of SCMAS aggregates in the same type of neurons, which are not statistically different from their WT counterparts (Figure 8B). These data are suggestive of CTSB involvement in amyloidogenesis in different types of neurological LSDs.

DISCUSSION

Despite many years of extensive research, no specific treatments have been clinically approved for MPS III and sialidosis. Moreover, as we currently know, gene therapy alone cannot reverse CNS pathology in symptomatic patients, emphasizing the need for the development of additional/alternative strategies—in particular, those using small-molecule drugs.[45,46] In the present work, we examined whether inhibition of CTSB, which we previously proposed to be responsible for the increased amyloidogenesis in neurological MPS diseases,[34] could ameliorate disease progression in MPS IIIC and sialidosis mouse models. Our data provide compelling evidence that secondary induction of CTSB in the pyramidal neurons contributes to the accumulation of amyloid deposits and misfolded proteins in the neurological lysosomal diseases MPS IIIC and sialidosis. We also demonstrate that by inhibiting CTSB activity, we can partially improve behavioral deficits and CNS pathology in MPS IIIC mice.

To establish a causative relation between the increased levels of CTSB and increased amyloidogenesis, we generated a knockin MPS IIIC mouse model with inactivated *Ctsb* gene (*Hgsnat*^{P304L}/*Ctsb*$^{-/-}$ strain). According to published studies, *Ctsb*$^{-/-}$ mice do not reveal severe neurological phenotypes or reduced lifespan, suggesting that CTSB function in the lysosome is somewhat redundant, and its deficiency can be partially compensated by other proteases.[47,48] We also treated MPS IIIC mice with an irreversible inhibitor of CTSB and other cysteine proteases, E64, at the dose and frequency previously reported to be sufficient to cause a sustainable inhibition of CTSB in the brain.[40–43] In both cases, we have observed a drastic reduction in β-amyloid^{+}/thioflavin S^{+} cytoplasmic aggregates in pyramidal neurons of deep cortical layers IV and V, the cells showing the highest levels of both amyloid deposits and CTSB immunolabeling in untreated *Hgsnat*^{P304L} mice and in *Hgsnat-Geo* mice, a KO model of MPS IIIC. Similar to our previous findings in *Idua*$^{-/-}$ MPS I mice,[34] CTSB shows a diffused labeling pattern in pyramidal cortical neurons of both sialidosis and MPS IIIC mice, which, together with the presence of GAL3C^{+} puncta in these neurons and increased CTSB content in the cytosol fraction from *Hgsnat*^{P304L} mouse brain tissues, is suggestive of CTSB leakage

Figure 5. Genetic inactivation of CTSB reduces levels of thioflavin S^{+}/β-amyloid^{+} aggregates and restores autophagic flux in cortical neurons of MPS IIIC mice

(A and B) CTSB immunoreacting material (A) and enzymatic activity (B) are not detected in cortical tissues of *Ctsb*$^{-/-}$ and *Hgsnat*^{P304L}/*Ctsb*$^{-/-}$ (double KO [DKO]) mice. (C) *Hgsnat*^{P304L} and *Hgsnat*^{P304L}/*Ctsb*$^{-/-}$ mice show increased levels and size of LAMP-2^{+} puncta in the neurons. (D) Six-month-old *Hgsnat*^{P304L} and *Hgsnat*^{P304L}/*Ctsb*$^{-/-}$ mice show similar levels of GFAP^{+} (green) and CD68^{+} (red) cells. (E) Storage of β-amyloid (red) and thioflavin-S^{+} misfolded proteins (Thio-S, green) is elevated in cortical neurons of 6-month-old *Hgsnat*^{P304L} mice but not in DKO *Hgsnat*^{P304L}/*Ctsb*$^{-/-}$ mice. (F–I) Genetic ablation of *Ctsb* reduces accumulation of G_{M2}-ganglioside (F), SCMAS (G), LC3^{+} (H), and p62^{+} (I) puncta in cortical neurons of *Hgsnat*^{P304L} mice. Bar graphs: 100 μm in (F), 15 μm in (H and I), and 25 μm in all other panels. Panels show representative confocal microscopy images of brain cortices (layers IV-V) of WT, *Ctsb*$^{-/-}$, *Hgsnat*^{P304L}, and *Hgsnat*^{P304L}/*Ctsb*$^{-/-}$ mice. Graphs show quantification of immunofluorescence with ImageJ software. Individual data, means, and SDs for five mice per genotype (three sections for each mouse) are shown. Statistical analysis was performed by nested ANOVA with the Tukey post hoc test.

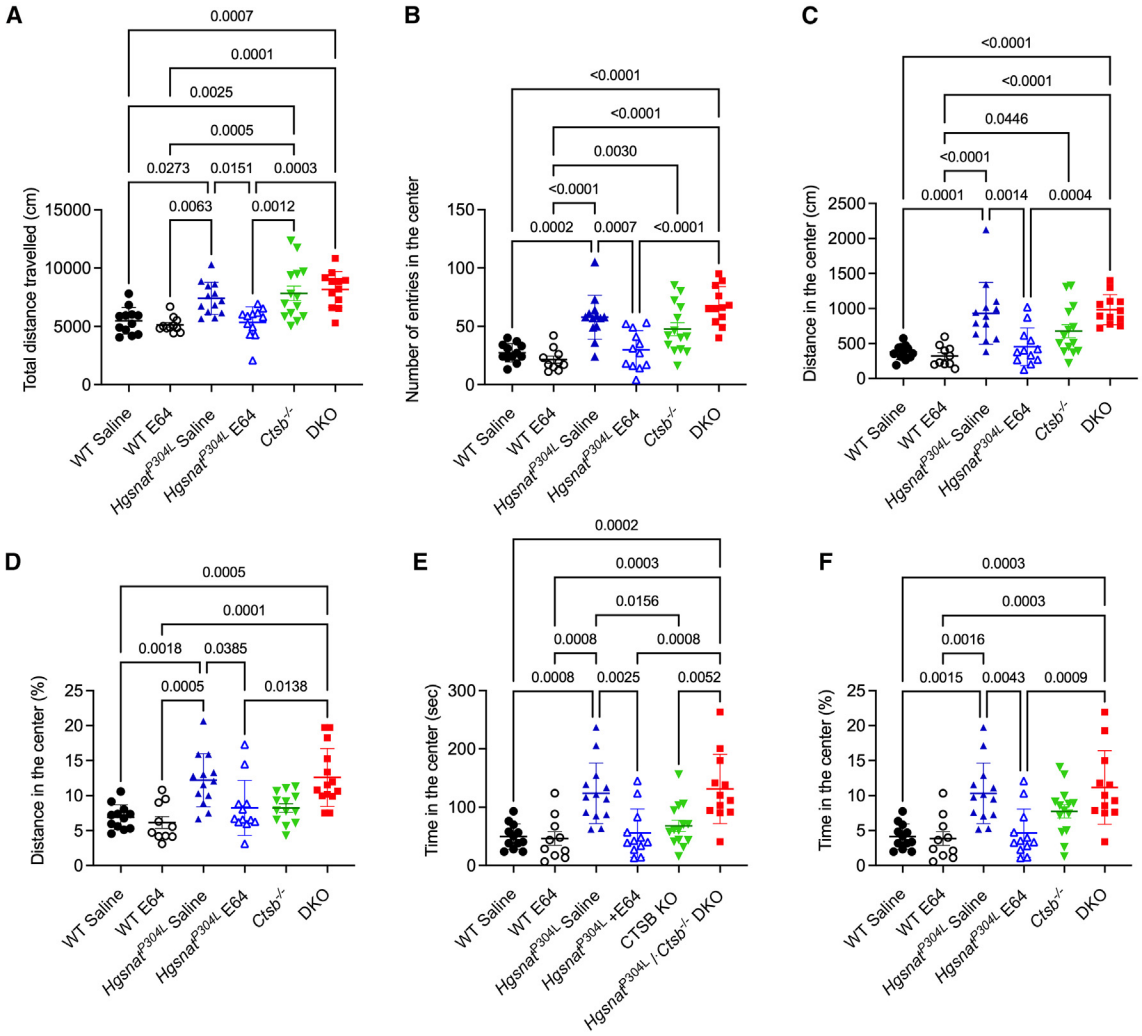

Figure 6. Thirty-day intranasal treatment with E64 rescues behavioral deficits in MPS IIIC mice

Hgsnat^{P304L} mice treated intranasally with E64 for 30 days at 1 mg/kg body weight (BW)/day show significant reduction of hyperactivity (A) and reduced anxiety (B–F) in the open field test at age 6 months compared with untreated *Hgsnat*^{P304L} mice. Double-deficient *Hgsnat*^{P304L}/*Ctsb*$^{-/-}$ mice show behavior similar to that of untreated *Hgsnat*^{P304L} mice. Individual results, means, and SDs from experiments performed with 10–14 mice per genotype per treatment are shown. *p* values were calculated by ANOVA with the Tukey post hoc test.

from the lysosome to the cytoplasm. In contrast to other lysosomal cysteine proteases, CTSB remains stable at neutral pH corresponding to that of the cytoplasm (reviewed in reference[49]). Moreover, a recent report demonstrates that CTSB, which mainly shows carboxypeptidase and dipeptidyl carboxypeptidase activities at the acidic pH of the lysosome, reveals endopeptidase activity at neutral pH,[50] which presumably allows the enzyme to conduct amylogenic processing of APP.

Notably, in the neurons of both E64-treated and *Ctsb*-depleted MPS IIIC mice, we also detected a drastic reduction in another secondary storage product, misfolded SCMAS protein, the accumulation of which has been previously associated with an autophagy block. In contrast to neurons of untreated *Hgsnat*^{P304L} mice, the cells in both E64-treated and CTSB KO *Hgsnat*^{P304L} mice did not display LC3^{+} and P62^{+} puncta, suggesting that CTSB depletion indeed rescued an autophagy flux. This is also consistent with the results of a recent study showing that CTSB regulates autophagy through the cleavage of the lysosomal calcium channel MCOLN1/TRPML1.[33]

At the same time, the effect of E64 treatment on behavioral abnormalities in *Hgsnat*^{P304L} mice was different from that of genetic *Ctsb* depletion. E64-treated mice demonstrated a rescue of hyperactivity and reduced anxiety characteristic of Sanfilippo disease mouse models.[12,13,35] In contrast, the *Hgsnat*^{P304L}/*Ctsb*$^{-/-}$ mice showed levels of hyperactivity and reduced anxiety similar to those of

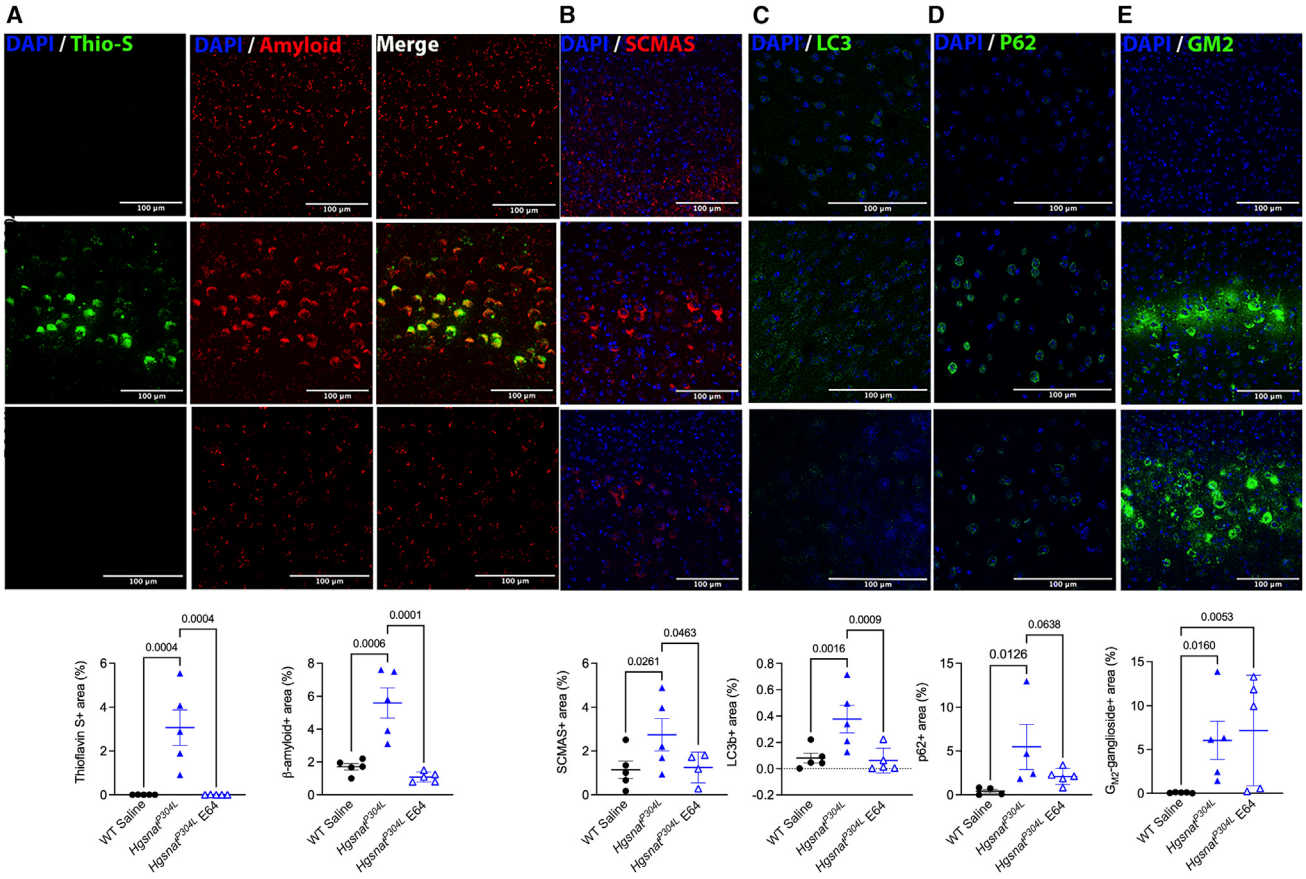

Figure 7. Thirty-day intranasal treatment with irreversible CTSB inhibitor E64 reduces levels of thioflavin S$^+$/β-amyloid$^+$ aggregates and restores autophagic flux in cortical neurons of MPS IIIC mice

(A) Accumulation of β-amyloid and misfolded proteins is not detected in cortical neurons of 6-month-old *Hgsnat*^{P304L} mice treated for 30 days with daily intranasal doses of E64 at 1 mg/kg BW. (B–D) E64 treatment reduces accumulation of SCMAS (B), LC3$^+$ (C), and p62$^+$ (D) puncta but not secondary storage of G_{M2}-ganglioside (E) in cortical neurons of *Hgsnat*^{P304L} mice. Panels show representative confocal microscopy images of brain cortices (layers IV-V) of WT, untreated *Hgsnat*^{P304L}, and E64-treated *Hgsnat*^{P304L} mice labeled for β-amyloid (A, red), thioflavin-S (A, green), SCMAS (B, red), LC3 (C, green), p62 (D, green), and G_{M2}-ganglioside (E, green). Graphs show quantification of immunofluorescence with ImageJ software. Individual data, means, and SDs are shown. Statistical analysis was performed by ANOVA with the Tukey post hoc test; *n* = 5 mice per genotype.

untreated *Hgsnat*^{P304L} mice. E64 treatment did not cause any changes in the behavior of control WT mice, ruling out the possibility that reduction of hyperactivity in the *Hgsnat*^{P304L} mice was caused by a sedative effect of the drug itself. Notably, while we do not see signs of CNS pathology characteristic of neurological LSDs, such as astrogliosis related to neuroinflammation or neuronal accumulation of gangliosides and ceroid materials in *Ctsb*$^{-/-}$ mice, their levels of hyperactivity and reduced anxiety were comparable to those of *Hgsnat*^{P304L} mice. Therefore, in the current experimental settings, it was impossible for us to conclude whether the above behavior deficits in *Hgsnat*^{P304L}/*Ctsb*$^{-/-}$ mice originated from CTSB genetic deficiency, HGSNAT deficiency, or both. Previously, CTSB genetic depletion has been shown to ameliorate behavioral deficits, neuropathology, and biomarkers in several mouse models of neurological diseases, including traumatic brain injury, ischemia, epilepsy, multiple sclerosis, opioid tolerance, and inflammatory pain (reviewed in reference[47]). At the same time, a recent study demonstrated that in iPSC-derived dopaminergic neurons, CTSB depletion reduced lysosomal glucocerebrosidase activity and impaired the degradation of pre-formed α-synuclein fibrils associated with pathogenesis in Parkinson disease.[51] Thus, the effect of CTSB reduction can be both positive and negative depending on the target cells and degree of depletion.

Our findings that treatment of MPS IIIC mice with the CTSB inhibitor E64 effectively prevents the accumulation of amyloid materials and rescues behavioral abnormalities positions this drug as a promising candidate for clinical translation in MPS IIIC and perhaps other neurological lysosomal diseases. Although the mechanism of the drug action needs further elucidation, the fact that it reduces the accumulation of secondary storage materials suggests that, in addition to blocking amyloidogenic cleavage of APP, E64 induces autophagy.

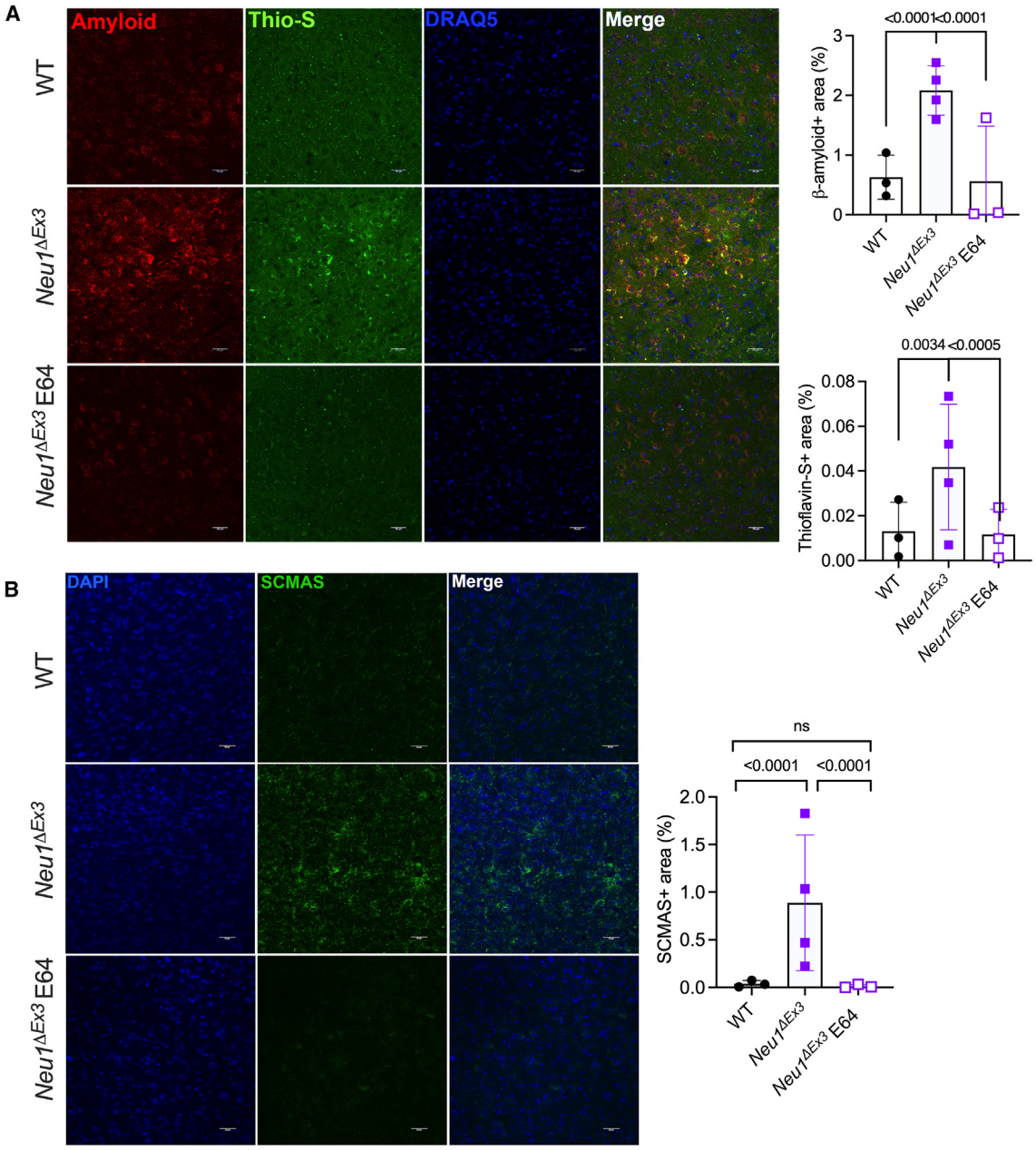

Figure 8. Thirty-day intranasal treatment with irreversible CTSB inhibitor E64 reduces levels of thioflavin S$^+$/β-amyloid$^+$ aggregates and misfolded SCMAS deposits in cortical neurons of sialidosis mice

(A) Storage of amyloidogenic peptides and misfolded proteins reduced in cortical neurons of 4-month-old *Neu1*$^{\Delta Ex3}$ mice treated for 60 days with daily intranasal doses of E64 at 1 mg/kg BW. (B) E64 treatment also reduces the accumulation of SCMAS in cortical neurons of *Neu1*$^{\Delta Ex3}$ mice. Panels show representative confocal microscopy images of brain cortices (layers IV-V) of WT, *Neu1*$^{\Delta Ex3}$, and E64-treated *Neu1*$^{\Delta Ex3}$ mice labeled for β-amyloid (A, red), thioflavin-S (A, green), and SCMAS (B, green). Nuclei were counterstained with Draq5 (A, blue) and DAPI (B, blue). Graphs show the quantification of immunofluorescence with ImageJ software. Individual data, means, and SDs are shown. Statistical analysis was performed by nested ANOVA with the Tukey post hoc test; $n = 3$–4 mice per genotype. Four brain sections were analyzed for each mouse.

The drug also reduced the expression of proinflammatory cytokine IL-1β, consistent with its role in the inflammasome activation (reviewed in reference[52]). At the same time, E64 treatment does not reduce astromicrogliosis and expression levels of two other proinflammatory cytokines, MIP1α and TNFα. Notably, a recent clinical trial demonstrated the improved neurobehavioral and functional outcomes in symptomatic MPS III patients undergoing anti-inflammatory therapy.[53] We hypothesize, therefore, that for an effective

treatment of progressive neuropathology, E64 needs to be used in combination with a therapy reducing neuroimmune response such as hematopoietic stem progenitor cell (HSPC) transplantation or HSPC gene therapy. Experiments aimed at testing this hypothesis are in progress in our laboratory. Previously E64 has shown efficacy in rescuing memory loss and reducing amyloid plaque formation in the AD mouse model,[43] demonstrated oral bioavailability, and has been approved by the US Food and Drug Administration for clinical trials. Pharmacological CTSB inhibitors also ameliorated neurodegeneration after traumatic brain injury,[54] retinopathy and optic neuritis in experimental autoimmune encephalomyelitis,[55] or HIV-1-induced neuronal damage.[56] In addition, potential indications for CTSB inhibiting drugs include other neurological and psychiatric diseases associated with increased CTSB levels such as amyotrophic lateral sclerosis, bipolar disorder, attention-deficit/hyperactivity disorder, and autism spectrum disorders (reviewed in references[47,52]).

Notably, multiple clinical trials involving enzyme replacement or gene therapy for MPS patients, both completed and ongoing, have yet to show efficacy for symptomatic patients, suggesting that correction of the enzymatic defect by itself cannot reverse or even halt the progression of neuronal pathology. Our current results showing that E64 administered by non-invasive intranasal route blocked amyloidogenesis in both symptomatic MPS IIIC and sialidosis mice justify further studies analyzing the efficacy of this compound for the treatment of neurological LSDs.

MATERIALS AND METHODS

Study approval

All animal experiments were approved by and performed in compliance with the Comité Institutionnel des Bonnes Pratiques Animales en Recherche (approval no. 2022-4353, approval date November 2023). Ethical approval for research involving human tissues was given by the CHU Ste-Justine Research Ethics Board (Comité d'Éthique de la Recherche FWA00021692, approval no. 2020-2365). The National Institutes of Health's NeuroBioBank provided the cerebral tissues, frozen or fixed with PFA, from MPS patients, as well as age-, ethnicity-, and sex-matched controls (project 1071, MPS Synapse), along with clinical descriptions and the results of a neuropathological examination.

Animals

The constitutive *Neu1* KO sialidosis mouse model $Neu1^{\Delta Ex3}$, the constitutive KO MPS IIIC mouse model *Hgsnat-Geo*, and the knockin MPS IIIC mouse model $Hgsnat^{P304L}$, expressing the HGSNAT enzyme with human missense mutation P304L, all in a C57BL/6J genetic background, have been previously described.[13,35,57] The strain of $Hgsnat^{P304L}/Ctsb^{-/-}$ mice was generated by breeding the $Hgsnat^{P304L}$ strain with previously described *Ctsb* KO mice obtained from The Jackson Laboratory (Jax strain [B6; 129-Ctsbtm1Jde/J]). Heterozygous mice were interbred, and litters were genotyped by PCR using genomic DNA extracted from clipped tail tips, as described. Mice homozygous for the mutant allele(s) were compared to appropriate age- and sex-matched WT control littermates. All mice were housed under 12-h/12-h light-dark cycles with *ad libitum* access to normal rodent chow and water.

Equal cohorts of male and female mice were studied separately for each experiment, and statistical methods were used to test whether the progression of the disease, levels of biomarkers, or response to therapy were different for male and female animals. Since differences between sexes were not detected, the data for male and female mice were pooled together.

Immunohistochemistry

Mouse brains were collected from animals, perfused with 4% PFA in PBS, and post-fixed in 4% PFA in PBS overnight. Brains were incubated in 30% sucrose for 2 days at 4°C, embedded in Tissue-Tek OCT Compound, cryopreserved, cut in 40-μm-thick sections, and stored in cryopreservation buffer (0.05 M sodium phosphate buffer, pH 7.4, 15% sucrose, 40% ethylene glycol) at −20°C pending immunohistochemistry. Mouse brain sections were washed three times with PBS and permeabilized/blocked by incubating in 5% bovine serum albumin (BSA), 0.3% Triton X-100 in PBS for 1 h at room temperature. Incubation with primary antibodies, diluted in 1% BSA, 0.3% Triton X-100 in PBS, was performed overnight at 4°C. The antibodies and their working concentrations are shown in Table S1. To conduct thioflavin-S staining, brain sections stained with Draq5, primary antibodies against β-amyloid, and Alexa Fluor-labeled secondary antibodies were washed three times with PBS and incubated in a 0.05% thioflavin-S (Sigma, T1892) solution in 50% ethanol/water for 10 min protected from light. Then, the sections were washed two times with 50% ethanol followed by two washes with double-distilled H_2O. The slides were mounted with Prolong Gold Antifade mounting reagent (Invitrogen, P36934) and analyzed using a Leica DM 5500 Q upright confocal microscope (10×, 40×, and 63× oil objective, numerical aperture 1.4). Autofluorescent ceroid materials in brain cortices were analyzed using mounted unstained tissue sections and confocal settings similar to those for GFP. Images were processed and quantified using ImageJ 1.50i software (NIH) in a blinded fashion. Panels were assembled with Adobe Photoshop.

Enzymatic assays and immunoblots

CTSB activity was measured using the fluorogenic Z-Arg-Arg-AMC substrate (Enzo Life Sciences) as described by Viana et al.[34] Levels of CTSB protein, total APPs, and C-terminal AP fragments (AP-CTF, antibodies 1–40 and antibodies 1–42 peptides together) were analyzed by immunoblots as previously described.[34]

Real-time qPCR

RNA was isolated from snap-frozen brain tissues using TRIzol reagent (Invitrogen) and reverse-transcribed using the Quantitect Reverse Transcription Kit (Qiagen, catalog no. 205311) according to the manufacturer's protocol. qPCR was performed using a LightCycler 96 Instrument (Roche) and SsoFast EvaGreen Supermix with Low ROX (Bio-Rad catalog no. 1725211) according to the manufacturer's protocol. The primers are shown in Table S2. The relative

levels of mRNA were calculated using the 2-ΔΔCt algorithm, with RLP32 mRNA as a reference control.

Subcellular fractionation of mouse brain tissues

Subcellular fractionation was performed essentially as described for the rat liver,[58] with the following modifications. Freshly harvested brains of three mice were homogenized in 3 volumes of 10 mM Tris-HCl buffer (pH 7.4) containing 250 mM sucrose, 1 mM EDTA, and a full protease inhibitor cocktail using a Potter-Elvehjem homogenizer (30 strokes, on ice). Nuclei and cell debris were removed by a 10-min centrifugation at 800 × *g*. Post-nuclear supernatant was further centrifuged for 30 min using an SW41-Ti Beckman rotor at 10,000 × *g* to collect the organellar pellet ("light mitochondrial fraction") containing lysosomes. The supernatant was further centrifuged using the same rotor for 2 h at 50,000 × *g* to separate the microsomal fraction (pellet) and cytosol. Aliquots of the post-nuclear supernatant, organellar pellet, and cytosol were analyzed by immunoblot as described above to determine the CTSB content.

Behavioral analysis

The OF test was performed as previously described.[59] Briefly, mice were habituated in the experimental room for 30 min before the commencement of the test. Each mouse was then gently placed in the center of the OF arena and allowed to explore for 20 min. The mouse was removed and transferred to its home cage after the test, and the arena was cleaned with 70% ethanol before the commencement of the next test. Analysis of the behavioral activity was done using Smart video tracking software (version 3.0, Panlab Harvard Apparatus); the total distance traveled and percentage of time spent in the center zone were measured for hyperactivity and anxiety assessment, respectively.

E64 treatment

Male and female 8- to 10-week-old C57BL/6 WT, *Hgsnat*^{P304L}, and *Neu1*$^{\Delta Ex3}$ mice were randomly assigned to either treatment (E64) or control (vehicle) groups each containing four to five male and female mice. Mice in the treatment group received daily intranasal administration of E64 (Sigma-Aldrich, catalog no. E3132) at a dose of 1 mg/kg BW dissolved in saline (0.9% sodium chloride). *Hgsnat*^{P304L} mice and their corresponding WT controls were treated for a duration of 1 month between 5 and 6 months of age. *Neu1*$^{\Delta Ex3}$ mice received the treatment for a duration of 2.5 months between the ages of 6 weeks and 4 months. The mice in the vehicle control groups received daily intranasal administration of saline. On treatment days, mice were gently restrained, and E64 solution or vehicle was administered intranasally using a micro-pipette. The administration volume was 5 μL per nostril, administered alternately. Care was taken to ensure uniformity in the administration technique across all animals. At the end of the 1-month treatment period, the mice were euthanized, and brain tissues harvested and processed for further analyses.

Statistical analysis

Statistical analyses were performed using Prism GraphPad 9.3.0 software. The normality for all data was analyzed using the D'Agostino-Pearson omnibus test. Significance of the difference was determined using t test (normal distribution) or the Mann-Whitney test, when comparing two groups. One-way ANOVA or nested ANOVA tests, followed by Tukey's multiple comparisons test (normal distribution), or the Kruskal-Wallis test, followed by Dunn's multiple comparisons test, were used when comparing more than two groups. Two-way ANOVA followed by Tukey's post hoc test was used for two-factor analysis. A $p \leq 0.05$ was considered significant.

DATA AVAILABILITY

The datasets used and/or analyzed during the present study are available from the corresponding author on reasonable request.

ACKNOWLEDGMENTS

The authors thank Dr. Christopher W. Cairo for a generous gift of fluorescently labeled GALC3 protein. We also are grateful to Elke Küster-Schöck and the Plateforme d'Imagerie Microscopique (PIM-CHU Sainte Justine) for the help with life imaging microscopy and Dr. Mila Ashmarina for critically reading the manuscript and helpful advice. This work has been partially supported by operating grants PJT-156345 and PJT-180546 from the Canadian Institutes of Health Research, research grant ND-1 from the Canadian Glycomics Network, the Elisa Linton Research Chair in Lysosomal Diseases, and a research grant co-funded by the Sanfilippo Children's Foundation and the Cure Sanfilippo Foundation to A.V.P. G.M.V. was partially supported by a Foreign Internship Scholarship (BEPE) from the Fundação de Amparo à Pesquisa do Estado de São Paulo (FAPESP). Approval for the animal experimentation was granted by the Animal Care and Use Committee of the CHU Sainte-Justine.

AUTHOR CONTRIBUTIONS

Conducted experiments and acquired data: G.M.V., X.P., S.F., T.X., and A.W.; analyzed data: G.M.V., X.P., S.F., T.X., and A.V.P.; provided essential resources: A.V.P.; wrote the manuscript (first draft): A.V.P., X.P., and G.M.V.; and edited the manuscript: X.P., G.M.V., and A.V.P. All authors read and approved the final manuscript.

DECLARATION OF INTERESTS

A.V.P. is a shareholder in and received honoraria and research contracts from Phoenix Nest, involved in the development of therapies for MPS IIID and IIIC.

SUPPLEMENTAL INFORMATION

Supplemental information can be found online at https://doi.org/10.1016/j.omtm.2025.101432.

REFERENCES

1. Giugliani, R. (2012). Newborn screening for lysosomal diseases: current status and potential interface with population medical genetics in Latin America. J. Inherit. Metab. Dis. *35*, 871–877.

2. Para, C., Bose, P., and Pshezhetsky, A.V. (2020). Neuropathophysiology of Lysosomal Storage Diseases: Synaptic Dysfunction as a Starting Point for Disease Progression. J. Clin. Med. *9*, 616.

3. Ebrahimi-Fakhari, D., Wahlster, L., Hoffmann, G.F., and Kölker, S. (2014). Emerging role of autophagy in pediatric neurodegenerative and neurometabolic diseases. Pediatr. Res. *75*, 217–226.

4. Ghavami, S., Shojaei, S., Yeganeh, B., Ande, S.R., Jangamreddy, J.R., Mehrpour, M., Christoffersson, J., Chaabane, W., Moghadam, A.R., Kashani, H.H., et al. (2014). Autophagy and apoptosis dysfunction in neurodegenerative disorders. Prog. Neurobiol. *112*, 24–49.

5. Yoon, S.Y., and Kim, D.H. (2016). Alzheimer's disease genes and autophagy. Brain Res. *1649*, 201–209.

6. Zhang, Y.D., and Zhao, J.J. (2015). TFEB Participates in the Abeta-Induced Pathogenesis of Alzheimer's Disease by Regulating the Autophagy-Lysosome Pathway. DNA Cell Biol. *34*, 661–668.

7. Cho, S.J., Yun, S.M., Jo, C., Lee, D.H., Choi, K.J., Song, J.C., Park, S.I., Kim, Y.J., and Koh, Y.H. (2015). SUMO1 promotes Abeta production via the modulation of autophagy. Autophagy *11*, 100–112.
8. Neufeld, E.F., and Muenzer, J. (2001). The mucopolysaccharidoses. In The Metabolic Basis of Inherited Disease, 8th ed. (McGraw-Hill), pp. 3421–3452.
9. Ohmi, K., Zhao, H.Z., and Neufeld, E.F. (2011). Defects in the medial entorhinal cortex and dentate gyrus in the mouse model of Sanfilippo syndrome type B. PLoS One *6*, e27461.
10. Pshezhetsky, A.V. (2016). Lysosomal storage of heparan sulfate causes mitochondrial defects, altered autophagy, and neuronal death in the mouse model of mucopolysaccharidosis III type C. Autophagy *12*, 1059–1060.
11. Beard, H., Hassiotis, S., Gai, W.P., Parkinson-Lawrence, E., Hopwood, J.J., and Hemsley, K.M. (2017). Axonal dystrophy in the brain of mice with Sanfilippo syndrome. Exp. Neurol. *295*, 243–255.
12. Wilkinson, F.L., Holley, R.J., Langford-Smith, K.J., Badrinath, S., Liao, A., Langford-Smith, A., Cooper, J.D., Jones, S.A., Wraith, J.E., Wynn, R.F., et al. (2012). Neuropathology in mouse models of mucopolysaccharidosis type I, IIIA and IIIB. PLoS One *7*, e35787.
13. Martins, C., Hůlková, H., Dridi, L., Dormoy-Raclet, V., Grigoryeva, L., Choi, Y., Langford-Smith, A., Wilkinson, F.L., Ohmi, K., DiCristo, G., et al. (2015). Neuroinflammation, mitochondrial defects and neurodegeneration in mucopolysaccharidosis III type C mouse model. Brain *138*, 336–355.
14. Ryazantsev, S., Yu, W.H., Zhao, H.Z., Neufeld, E.F., and Ohmi, K. (2007). Lysosomal accumulation of SCMAS (subunit c of mitochondrial ATP synthase) in neurons of the mouse model of mucopolysaccharidosis III B. Mol. Genet. Metabol. *90*, 393–401.
15. Ohmi, K., Greenberg, D.S., Rajavel, K.S., Ryazantsev, S., Li, H.H., and Neufeld, E.F. (2003). Activated microglia in cortex of mouse models of mucopolysaccharidoses I and IIIB. Proc. Natl. Acad. Sci. USA *100*, 1902–1907.
16. Dawson, G., Fuller, M., Helmsley, K.M., and Hopwood, J.J. (2012). Abnormal gangliosides are localized in lipid rafts in Sanfilippo (MPS3a) mouse brain. Neurochem. Res. *37*, 1372–1380.
17. Pierzynowska, K., Gaffke, L., Podlacha, M., Brokowska, J., and Węgrzyn, G. (2020). Mucopolysaccharidosis and Autophagy: Controversies on the Contribution of the Process to the Pathogenesis and Possible Therapeutic Applications. NeuroMolecular Med. *22*, 25–30.
18. Scarcella, M., Scerra, G., Ciampa, M., Caterino, M., Costanzo, M., Rinaldi, L., Feliciello, A., Anzilotti, S., Fiorentino, C., Renna, M., et al. (2024). Metabolic rewiring and autophagy inhibition correct lysosomal storage disease in mucopolysaccharidosis IIIB. iScience *27*, 108959.
19. Maeda, M., Seto, T., Kadono, C., Morimoto, H., Kida, S., Suga, M., Nakamura, M., Kataoka, Y., Hamazaki, T., and Shintaku, H. (2019). Autophagy in the Central Nervous System and Effects of Chloroquine in Mucopolysaccharidosis Type II Mice. Int. J. Mol. Sci. *20*, 5829.
20. Capuozzo, A., Montefusco, S., Cacace, V., Sofia, M., Esposito, A., Napolitano, G., Nusco, E., Polishchuk, E., Pizzo, M.T., De Risi, M., et al. (2022). Fluoxetine ameliorates mucopolysaccharidosis type IIIA. Mol. Ther. *30*, 1432–1450.
21. Annunziata, I., Patterson, A., Helton, D., Hu, H., Moshiach, S., Gomero, E., Nixon, R., and d'Azzo, A. (2013). Lysosomal NEU1 deficiency affects amyloid precursor protein levels and amyloid-beta secretion via deregulated lysosomal exocytosis. Nat. Commun. *4*, 2734.
22. Haass, C., Kaether, C., Thinakaran, G., and Sisodia, S. (2012). Trafficking and proteolytic processing of APP. Cold Spring Harb. Perspect. Med. *2*, a006270.
23. Li, R., Lindholm, K., Yang, L.B., Yue, X., Citron, M., Yan, R., Beach, T., Sue, L., Sabbagh, M., Cai, H., et al. (2004). Amyloid beta peptide load is correlated with increased beta-secretase activity in sporadic Alzheimer's disease patients. Proc. Natl. Acad. Sci. USA *101*, 3632–3637.
24. Fukumoto, H., Cheung, B.S., Hyman, B.T., and Irizarry, M.C. (2002). Beta-secretase protein and activity are increased in the neocortex in Alzheimer disease. Arch. Neurol. *59*, 1381–1389.
25. Hook, V., Schechter, I., Demuth, H.U., and Hook, G. (2008). Alternative pathways for production of beta-amyloid peptides of Alzheimer's disease. Biol. Chem. *389*, 993–1006.
26. Hook, V., Toneff, T., Bogyo, M., Greenbaum, D., Medzihradszky, K.F., Neveu, J., Lane, W., Hook, G., and Reisine, T. (2005). Inhibition of cathepsin B reduces beta-amyloid production in regulated secretory vesicles of neuronal chromaffin cells: evidence for cathepsin B as a candidate beta-secretase of Alzheimer's disease. Biol. Chem. *386*, 931–940.
27. Chevallier, N., Vizzavona, J., Marambaud, P., Baur, C.P., Spillantini, M., Fulcrand, P., Martinez, J., Goedert, M., Vincent, J.P., and Checler, F. (1997). Cathepsin D displays in vitro beta-secretase-like specificity. Brain Res. *750*, 11–19.
28. Di Domenico, F., Coccia, R., Cocciolo, A., Murphy, M.P., Cenini, G., Head, E., Butterfield, D.A., Giorgi, A., Schinina, M.E., Mancuso, C., et al. (2013). Impairment of proteostasis network in Down syndrome prior to the development of Alzheimer's disease neuropathology: redox proteomics analysis of human brain. Biochim. Biophys. Acta *1832*, 1249–1259.
29. Sun, B., Zhou, Y., Halabisky, B., Lo, I., Cho, S.H., Mueller-Steiner, S., Devidze, N., Wang, X., Grubb, A., and Gan, L. (2008). Cystatin C-cathepsin B axis regulates amyloid beta levels and associated neuronal deficits in an animal model of Alzheimer's disease. Neuron *60*, 247–257.
30. Wu, Z., Sun, L., Hashioka, S., Yu, S., Schwab, C., Okada, R., Hayashi, Y., McGeer, P.L., and Nakanishi, H. (2013). Differential pathways for interleukin-1beta production activated by chromogranin A and amyloid beta in microglia. Neurobiol. Aging *34*, 2715–2725.
31. Qiao, C., Yin, N., Gu, H.Y., Zhu, J.L., Ding, J.H., Lu, M., and Hu, G. (2016). Atp13a2 Deficiency Aggravates Astrocyte-Mediated Neuroinflammation via NLRP3 Inflammasome Activation. CNS Neurosci. Ther. *22*, 451–460.
32. Ni, J., Wu, Z., Stoka, V., Meng, J., Hayashi, Y., Peters, C., Qing, H., Turk, V., and Nakanishi, H. (2019). Increased expression and altered subcellular distribution of cathepsin B in microglia induce cognitive impairment through oxidative stress and inflammatory response in mice. Aging Cell *18*, e12856.
33. Man, S.M., and Kanneganti, T.D. (2016). Regulation of lysosomal dynamics and autophagy by CTSB/cathepsin B. Autophagy *12*, 2504–2505.
34. Viana, G.M., Gonzalez, E.A., Alvarez, M.M.P., Cavalheiro, R.P., do Nascimento, C.C., Baldo, G., D'Almeida, V., de Lima, M.A., Pshezhetsky, A.V., and Nader, H.B. (2020). Cathepsin B-associated Activation of Amyloidogenic Pathway in Murine Mucopolysaccharidosis Type I Brain Cortex. Int. J. Mol. Sci. *21*, 1459.
35. Pan, X., Taherzadeh, M., Bose, P., Heon-Roberts, R., Nguyen, A.L.A., Xu, T., Pará, C., Yamanaka, Y., Priestman, D.A., Platt, F.M., et al. (2022). Glucosamine amends CNS pathology in mucopolysaccharidosis IIIC mouse expressing misfolded HGSNAT. J. Exp. Med. *219*, e20211860.
36. Kho, I., Demina, E.P., Pan, X., Londono, I., Cairo, C.W., Sturiale, L., Palmigiano, A., Messina, A., Garozzo, D., Ung, R.V., et al. (2023). Severe kidney dysfunction in sialidosis mice reveals an essential role for neuraminidase 1 in reabsorption. JCI Insight *8*, e166470.
37. Lowden, J.A., and O'Brien, J.S. (1979). Sialidosis: a review of human neuraminidase deficiency. Am. J. Hum. Genet. *31*, 1–18.
38. Pshezhetsky, A.V., Richard, C., Michaud, L., Igdoura, S., Wang, S., Elsliger, M.A., Qu, J., Leclerc, D., Gravel, R., Dallaire, L., and Potier, M. (1997). Cloning, expression and chromosomal mapping of human lysosomal sialidase and characterization of mutations in sialidosis. Nat. Genet. *15*, 316–320.
39. Yang, E.H., Rode, J., Howlader, M.A., Eckermann, M., Santos, J.T., Hernandez Armada, D., Zheng, R., Zou, C., and Cairo, C.W. (2017). Galectin-3 alters the lateral mobility and clustering of beta1-integrin receptors. PLoS One *12*, e0184378.
40. Hook, V.Y.H., Kindy, M., and Hook, G. (2008). Inhibitors of cathepsin B improve memory and reduce beta-amyloid in transgenic Alzheimer disease mice expressing the wild-type, but not the Swedish mutant, beta-secretase site of the amyloid precursor protein. J. Biol. Chem. *283*, 7745–7753.
41. Hook, V., Hook, G., and Kindy, M. (2010). Pharmacogenetic features of cathepsin B inhibitors that improve memory deficit and reduce beta-amyloid related to Alzheimer's disease. Biol. Chem. *391*, 861–872.
42. Hook, G., Jacobsen, J.S., Grabstein, K., Kindy, M., and Hook, V. (2015). Cathepsin B is a New Drug Target for Traumatic Brain Injury Therapeutics: Evidence for E64d as a Promising Lead Drug Candidate. Front. Neurol. *6*, 178.
43. Hook, G., Hook, V., and Kindy, M. (2011). The cysteine protease inhibitor, E64d, reduces brain amyloid-beta and improves memory deficits in Alzheimer's disease

animal models by inhibiting cathepsin B, but not BACE1, beta-secretase activity. J. Alzheimers Dis. *26*, 387–408.

44. Dhuyvetter, D., Tekle, F., Nazarov, M., Vreeken, R.J., Borghys, H., Rombouts, F., Lenaerts, I., and Bottelbergs, A. (2020). Direct nose to brain delivery of small molecules: critical analysis of data from a standardized in vivo screening model in rats. Drug Deliv. *27*, 1597–1607.

45. Biffi, A., Montini, E., Lorioli, L., Cesani, M., Fumagalli, F., Plati, T., Baldoli, C., Martino, S., Calabria, A., Canale, S., et al. (2013). Lentiviral hematopoietic stem cell gene therapy benefits metachromatic leukodystrophy. Science *341*, 1233158.

46. Sessa, M., Lorioli, L., Fumagalli, F., Acquati, S., Redaelli, D., Baldoli, C., Canale, S., Lopez, I.D., Morena, F., Calabria, A., et al. (2016). Lentiviral haemopoietic stem-cell gene therapy in early-onset metachromatic leukodystrophy: an ad-hoc analysis of a non-randomised, open-label, phase 1/2 trial. Lancet *388*, 476–487.

47. Hook, G., Reinheckel, T., Ni, J., Wu, Z., Kindy, M., Peters, C., and Hook, V. (2022). Cathepsin B Gene Knockout Improves Behavioral Deficits and Reduces Pathology in Models of Neurologic Disorders. Pharmacol. Rev. *74*, 600–629.

48. Moon, H.Y., Becke, A., Berron, D., Becker, B., Sah, N., Benoni, G., Janke, E., Lubejko, S.T., Greig, N.H., Mattison, J.A., et al. (2016). Running-Induced Systemic Cathepsin B Secretion Is Associated with Memory Function. Cell Metab. *24*, 332–340.

49. Turk, V., Stoka, V., Vasiljeva, O., Renko, M., Sun, T., Turk, B., and Turk, D. (2012). Cysteine cathepsins: from structure, function and regulation to new frontiers. Biochim. Biophys. Acta *1824*, 68–88.

50. Yoon, M.C., Hook, V., and O'Donoghue, A.J. (2022). Cathepsin B Dipeptidyl Carboxypeptidase and Endopeptidase Activities Demonstrated across a Broad pH Range. Biochemistry *61*, 1904–1914.

51. Jones-Tabah, J., He, K., Senkevich, K., Karpilovsky, N., Deyab, G., Cousineau, Y., Nikanorova, D., Goldsmith, T., Del Cid Pellitero, E., Chen, C.X., et al. (2023). The Parkinson's disease risk gene cathepsin B promotes fibrillar alpha-synuclein clearance, lysosomal function and glucocerebrosidase activity in dopaminergic neurons. Preprint at bioRxiv. https://doi.org/10.1101/2023.11.11.566693.

52. Ni, J., Lan, F., Xu, Y., Nakanishi, H., and Li, X. (2022). Extralysosomal cathepsin B in central nervous system: Mechanisms and therapeutic implications. Brain Pathol. *32*, e13071.

53. Polgreen, L.E., Chen, A.H., Pak, Y., Luzzi, A., Morales Garval, A., Acevedo, J., Bitan, G., Iacovino, M., O'Neill, C., and Eisengart, J.B. (2024). Author Correction: Anakinra in Sanfilippo syndrome: a phase 1/2 trial. Nat. Med. *30*, 2693.

54. Luo, C.L., Chen, X.P., Yang, R., Sun, Y.X., Li, Q.Q., Bao, H.J., Cao, Q.Q., Ni, H., Qin, Z.H., and Tao, L.Y. (2010). Cathepsin B contributes to traumatic brain injury-induced cell death through a mitochondria-mediated apoptotic pathway. J. Neurosci. Res. *88*, 2847–2858.

55. Rashid Khan, M., Fayaz Ahmad, S., Nadeem, A., Imam, F., Al-Harbi, N.O., Shahnawaz Khan, M., Alsahli, M., and Alhosaini, K. (2023). Cathepsin-B inhibitor CA-074 attenuates retinopathy and optic neuritis in experimental autoimmune encephalomyelitis induced in SJL/J mice. Saudi Pharm. J. *31*, 147–153.

56. Zenon-Melendez, C.N., Carrasquillo Carrion, K., Cantres Rosario, Y., Roche Lima, A., and Melendez, L.M. (2022). Inhibition of Cathepsin B and SAPC Secreted by HIV-Infected Macrophages Reverses Common and Unique Apoptosis Pathways. J. Proteome Res. *21*, 301–312.

57. Pan, X., De Aragão, C.D.B.P., Velasco-Martin, J.P., Priestman, D.A., Wu, H.Y., Takahashi, K., Yamaguchi, K., Sturiale, L., Garozzo, D., Platt, F.M., et al. (2017). Neuraminidases 3 and 4 regulate neuronal function by catabolizing brain gangliosides. FASEB J. *31*, 3467–3483.

58. Evans, W.H. (1992). Isolation and characterization of membranes and cell organelles. In PreparativeCentrifugation - A Practical Approach, D. Rickwood, ed. (Oxford University Press), pp. 233–270.

59. Amegandjin, C.A., Choudhury, M., Jadhav, V., Carriço, J.N., Quintal, A., Berryer, M., Snapyan, M., Chattopadhyaya, B., Saghatelyan, A., and Di Cristo, G. (2021). Sensitive period for rescuing parvalbumin interneurons connectivity and social behavior deficits caused by TSC1 loss. Nat. Commun. *12*, 3653.